Pyroelectricity of Benzene Derivates.
II. Metanitrochlorobenzene, Paranitrobenzonitrile, and Parabromobenzonitrile

Silvia Fleck * and Alarich Weiss

Institut für Physikalische Chemie, Physikalische Chemie III,
Technische Hochschule Darmstadt, Darmstadt, West Germany

The pyroelectric properties of the benzene derivatives, $1\text{-Cl-}3\text{-NO}_2\text{-C}_6\text{H}_4$, $1\text{-CN-}4\text{-NO}_2\text{-C}_6\text{H}_4$, and $1\text{-CN-}4\text{-Br-C}_6\text{H}_4$, were investigated in the temperature range $100 \leqq T/K \leqq$ decomposition temperature. Dielectric measurements of single crystals of these compounds were performed. By use of a semiempirical quantum chemical model, including a point charge model of the solid matrix, the charge distributions in the molecules are calculated. With the therefrom resulting dipole moment and properties of a polar dielectric the change of the pyroelectric coefficient p with temperature is calculated. The experiments and calculations are discussed in connection with the known crystal structures of the substances.

Introduction

Polar crystals showing very large pyroelectric coefficients are found as well among inorganic solids as organic salts. Strong polarizability and/or hydrogen bonds within these classes of solids can be of advantage for strong pyroelectricity.

There is a third class of solids which deserves attention with respect to the phenomenon of pyroelectricity. This comprises organic molecular crystals, particularly benzene derivatives, composed of molecules which crystallize in a polar crystal class and may have an easy polarizable π-system of electrons. We have recently reported on the pyroelectricity of $1\text{-NH}_2\text{-}3\text{-NO}_2\text{-C}_6\text{H}_4$, $1\text{-OH-}3\text{-NH}_2\text{-C}_6\text{H}_4$, and $1\text{-OH-}2{,}3\text{-Cl}_2\text{-C}_6\text{H}_3$ [1].

Large single crystals are needed for measurements of the pyroelectric coefficient of a solid. We have been able to grow large single crystals of m-chloronitrobenzene (CNB), $1\text{-Cl-}3\text{-NO}_2\text{-C}_6\text{H}_4$, p-nitrobenzonitrile (NBN), $1\text{-CN-}4\text{-NO}_2\text{-C}_6\text{H}_4$, and p-bromobenzonitrile (BBN), $1\text{-CN-}4\text{-Br-C}_6\text{H}_4$. The relatively simple molecular structure of these three compounds allows a comparison between pyroelectricity and molecular properties. CNB, NBN, and BBN crystallize in the space groups $C_{2v}^9\text{-Pna2}_1$, $C_2^2\text{-P2}_1$, and $C_s^3\text{-Cm}$, respectively [2−4]. Therefrom it is seen that BBN has a pyroelectric coefficient which can point in any direction within the ac-plane of the crystal, $\boldsymbol{p} = (p_1\,0\,p_3)$. Such a behaviour has been studied for example on the ferroelectric lithium trihydrogen selenite [5] and on ammonium hydrogen-DL-malate monohydrate [6]. The other two compounds, CNB and NBN, show a polarization along the axis [001], $\boldsymbol{p} = (0\,0\,p_3)$, and along the axis [010], $\boldsymbol{p} = (0\,p_2\,0)$, respectively. For $1\text{-Cl-}3\text{-NO}_2\text{-C}_6\text{H}_4$ the single crystal $^{35}\text{Cl-NQR}$ spectrum was studied, together with the crystal structure, in detail [2].

Experimental

Preparation

The compounds CNB, NBN, and BBN used for the growth of single crystals were of commercial source (purity $> 98\%$). CNB was further purified by crystallization from ethanolic solution. Single crystals were obtained by cooling a saturated ethanolic solution from $T \cong 308$ K down to room temperature; melting point (T_m) of CNB $= 318$ K. Large single crystals of this compound have been grown recently for ^{35}Cl single crystal NQR-spectroscopy [2]. The crystal axis could be identified by comparing the measurements on the optical goniometer with the crystal structure data. Crystal plates

---

parallel to the (001) plane with an area $13 \leqq A/mm^2 \leqq 25$ and thickness $0.7 \leqq d/mm \leqq 1.0$ were cut with a wire saw.

NBN was purified by sublimation under reduced pressure, and by chance a large single crystal was obtained during this procedure ($T_m = 421$ K). The crystals of NBN show a perfect cleavage plane, which contains the polar axis [010]. Within the cleavage plane the direction of the polar axis was identified by pyroelectric measurements. Than crystal plates perpendicular to [010] with an area $9 \leqq A/mm^2 \leqq 15$ and thickness $0.9 \leqq d/mm \leqq 1.1$ were cut. We have not been able to produce larger plates because of the ease of cleavage. From ethanolic solution small plates grow which are elongated along the polar axis.

The third substance discussed here, BBN, was purified by zone melting and single crystals could be obtained by this method ($T_m = 386$ K). The orientation of the axes of the single crystal was determined by X-ray diffraction. Crystal plates with the zone axis [010] and varying orientation of their normal with respect to [100] and with dimensions $16 \leqq A/mm^2 \leqq 60$ and $0.7 \leqq d/mm \leqq 1.1$ were cut.

For the measurement of the dielectric constants and the pyroelectric coefficients of CNB, NBN, and BBN, crystal plates prepared in the way described above, were polished and painted at the two opposite large faces with an air drying silver paste. In this way single crystal capacitors for the experiments were obtained [7].

Measurements of the Dielectric Constants and the Pyroelectric Coefficients

The complex dielectric constant, $\varepsilon = \varepsilon' - i\,\varepsilon''$, was found from impedance measurements of oriented single crystal capacitors, applying a bridge method described in [7]. The temperature range covered was $200 \leqq T/K \leqq T_d$ (T_d = decomposition temperature). Quite below the melting point, due to sublimation disturbances in the measurements occurred. This influences the accuracy of the dielectric measurements in the case of CNB, $\Delta\varepsilon = \pm 5\%$. In the case of NBN only elongated crystal plates were available, and again $\Delta\varepsilon = \pm 5\%$. The dielectric constant of BBN is accurate to $\pm 3\%$.

The temperature dependence of the pyroelectric coefficient at constant stress was measured in two different ways as described in [1, 7]. Either the

single crystal capacitor is heated or cooled with a constant rate, $0.5 \leqq \Delta T \cdot \Delta t^{-1}/(K \cdot min^{-1}) \leqq 4$. The resulting pyroelectric current is than measured by means of a shunt resistance ($10^{10}\,\Omega$) and an ultra high impedance electrometer. In the second way the temperature of the sample is varied sinusoidal and the pyroelectric coefficient is calculated from the responding sinusoidal pyroelectric current. The second method was not employed in case of NBN because the pyroelectric coefficient was too small to be determined thereby reliably.

The pyroelectric coefficients of the three substances under investigation were studied on several individual crystal plates for each compound. The temperature range $100 \leqq T/K \leqq T_d$ was covered and an accuracy of $\pm 10\%$ in $|p|$ was obtained.

Results

Dielectric Constants

The complex dielectric constants, $\varepsilon = \varepsilon' - i\,\varepsilon''$, of CNB and NBN were measured in the direction of the polar axes only. The component of the dielectric tensor, ε'_{33}, of CNB shows a steady increase in the range $200 \leqq T/K \leqq 310$ from 3.6 to 4, and $d\varepsilon'/dT$ increases with T, see Figure 1. The steep increase of ε'_{33} above 306 K is due to an onset of decomposition.

The component of the dielectric tensor in the direction of the polar axis of NBN, ε'_{22}, is comparable to that of CNB, but the temperature dependence is quite different (Figure 2). While ε'_{22} rises from 3.4 to 3.9 in the range $200 \leqq T/K \leqq 340$, $d\varepsilon'_{22}/dT$ decreases with T. A maximum of ε'_{22} at about 340 K appears. Thereafter $d\varepsilon'/dT$ is negative and the slope grows with T. At about 380 K cracks appear in the single crystals of NBN making measurements of the dielectric constant for $T > 395\,K$ useless.

In the case of BBN the whole dielectric tensor (ε_{ij}) was studied, $i, j = 1, 2, 3$; $\varepsilon_{ij} = \varepsilon_{ji}$; $\varepsilon_{12}, \varepsilon_{23} = 0$. ε_{22} can be measured directly on (010)-crystal plates (curve V in Figure 3). The other three tensor components, ε_{11}, ε_{13}, and ε_{33}, describe an ellipse in the ac-plane of the crystal. They have been calculated from measurements of the dielectric constant in different directions in the ac-plane (curves I–IV in Fig. 3) as described in [6, 8]. The resulting dielectric tensor does not change, neither in orientation nor in magnitude of the components, in the investigated
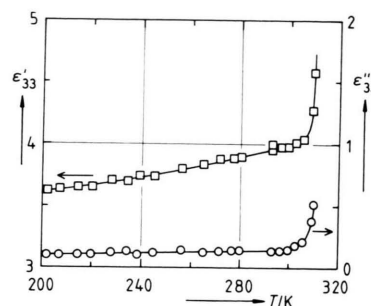
Fig. 1. Dielectric constant ε'_{33} ($\square$), ε''_{33} ($\bigcirc$) in the direction of the polar axis 2_1 of 1-Cl-3-NO_2-C_6H_4 vs. temperature.
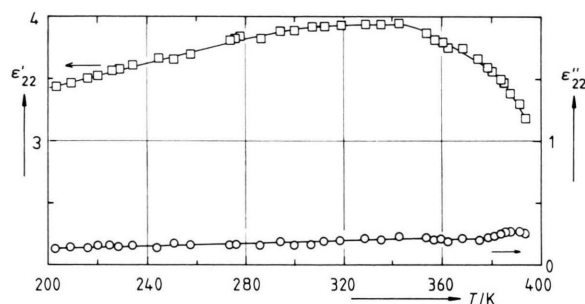
Fig. 2. Dielectric constant ε'_{22} ($\square$), ε''_{22} ($\bigcirc$) in the direction of the polar axis 2_1 of 1-CN-4-NO_2-C_6H_4 vs. temperature.
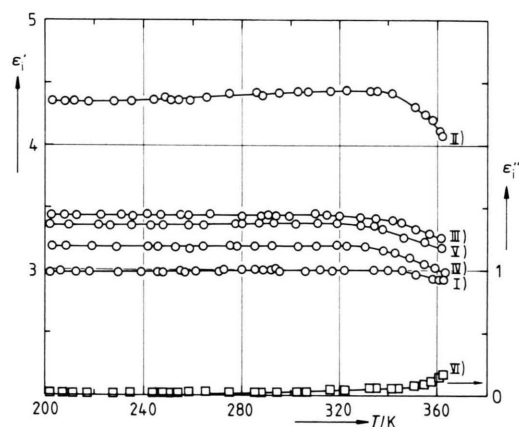
Fig. 3. Components of the dielectric constant in the ac-plane of 1-CN-4-Br-C_6H_4, ε'_i ($\bigcirc$), characterized by θ = angle between the axis [100] and the direction of measurement vs. temperature. I)–IV): I) $\theta_I = 109°$; II) $\theta_{II} = 19°$; III) $\theta_{III} = 74°$; IV) $\theta_{IV} = 141°$; V) corresponds to the measurement on a plate cut parallel to the plane (010), ε''_{22}. VI) ε'' ($\square$) corresponding to all directions.
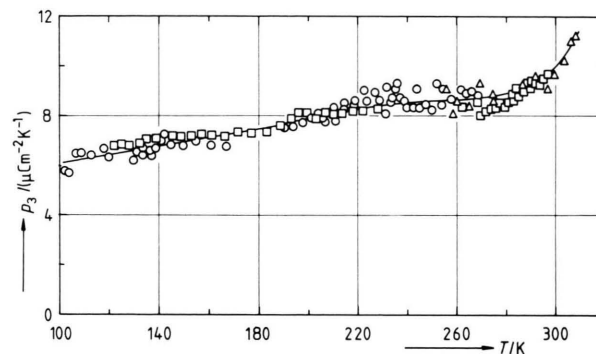

Fig. 4. Pyroelectric coefficient of 1-Cl-3-NO_3-C_6H_4, p_3, vs. temperature. Squares represent measurements done with increasing temperature, circles with decreasing temperature, and triangles with sinusoidal temperature oscillation.
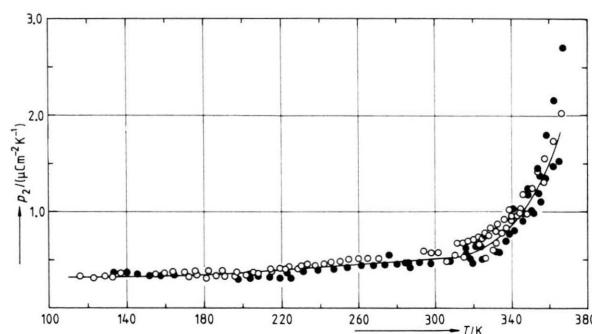

Fig. 5. Pyroelectric coefficient of 1-CN-4-NO_2-C_6H_4, p_2, vs. temperature. Full circles represent measurements done with increasing temperature, open ones with decreasing temperature.

temperature range up to 340 K: $\varepsilon_{11} = 3.14$; $\varepsilon_{13} = 0.52$; $\varepsilon_{33} = 4.17$; $\varepsilon_{22} = 3.38$. The dielectric tensor in the principal coordinate system found by the circle construction of Mohr [8] reads: $\varepsilon_{11} = 2.93$; $\varepsilon_{22} = 3.38$; $\varepsilon_{33} = 4.39$. The angle Φ between the principal axis of the dielectric ellipse in the ac-plane and the crystallographic axis [100] is 22.6°. For temperatures > 340 K the dielectric constant decreases.

Pyroelectric Coefficient

The pyroelectric coefficients at constant stress of the three substances under investigation have been determined in the temperature range $100 \leqq T/K \leqq T_d$. The temperature dependences of p_3(CNB) and p_2(NBN) are shown in Figs. 4 and 5, respectively. Both curves exhibit an increasing $|p|$ with increasing temperature, despite the fact that p_3(CNB) $\cong 20 \cdot p_2$(NBN) for $100 \leqq T/K \leqq 300$. For
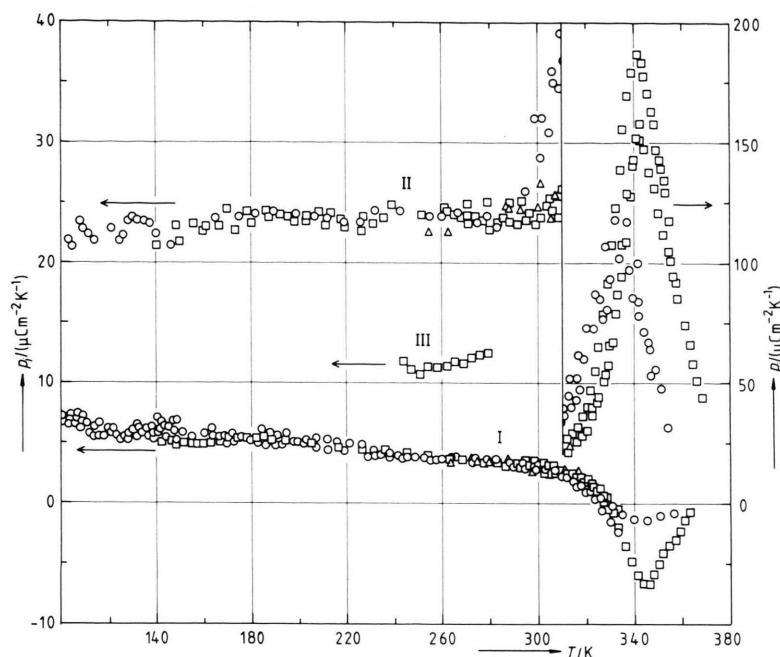
Fig. 6. Components of the pyro-electric vector, p_i, in different directions within the ac-plane of 1-CN-4-Br-C_6H_4 characterized by θ_i, vs. temperature. θ_i is defined as in legend to Fig. 3: I) $\theta_I = 109°$; II) $\theta_{II} = 19°$; III) $\theta_{III} = 74°$. The squares represent measurements done with increasing temperature, circles correspond to decreasing temperature. The data points obtained by use of sinusoidal temperature oscillation method are labeled by triangles.

temperatures > 300 K the curvature of p_3(CNB) steepens due to onset of decomposition.

For p_2(NBN) a pronounced increase of p_2 with raising T is found, too. The increase starts at $T = 320$ K and apparent values of $p_2 \cong 50$ μC m^{-2} K^{-1} at $T \cong 380$ K (not shown in Fig. 5) have been registered. After heating to $T < 380$ K the curve displayed in Fig. 5 can be reproduced on cooling. This is not possible if the sample is heated above 380 K. Disturbances due to cracks in the crystals appear and measurements of the pyroelectric coefficient have been found to be of no further use. NBN was studied by differential thermal analysis (DTA), too, and both on heating and cooling a phase transition at $T_c = 386$ K was found. Obviously the phase transition is reversible but accompanied by volume changes which give rise to cracks in the crystals. The decrease of ε'_{22} and the discontinuity of p_2(NBN) $= f(T)$ at about $T = 380$ K are in accordance with T_c found from DTA.

$|p|$ of BBN was found from independent measurements of the pyroelectric coefficient in two directions orthogonal to each other within the ac-plane (Fig. 6), the directions being characterized by θ, the angle between the direction of measurement and the axis [100]. For an unambiguous assignment of the direction of p a measurement in a third direction

was done for $240 \leq T/K \leq 280$, the sign being still undetermined. Both, the absolute value and the direction of p, characterized by ψ, the angle between p and the axis [100], are shown in Figure 7.

$|p|$ of BBN is almost constant for $100 \leq T/K \leq 320$, exhibiting the largest pyroelectric coefficient of the three substances investigated. Above 320 K a maximum of the pyroelectric coefficient is found, reaching $|p|_{max} \cong 7 \cdot |p|_{100 \leq T/K \leq 300}$. The temperature of $|p|_{max}$, T_{max}, was determined by the method of constant temperature change. In heating cycles $T_{max} \cong 343$ K and in cooling cycles $T_{max} \cong 333$ K. Whether $|p|$ goes to zero for $T > T_{max}$ and the origin of the maximum in $|p|$ is a phase transition could not be proved. DTA does not show any enthalpy effect and $T_m = 386$ K is reached within the observed decay range of p(BBN). Currents of non pyroelectric origin appear if the crystal is kept at $T = 375$ K for about 10 min. Thereafter the curve $p = f(T)$ is not reproducible. Sublimation is one possible source of this behaviour.

Furthermore for BBN, symmetry m, a strong angular dependence $p = f(\psi)$ is observed with a nearly constant $d\psi/dT$ in the range $100 \leq T/K \leq 300$ from $\psi = 2.5°$ to $\psi = 11.5°$. Thereafter the curvature of $\psi = f(T)$ steepens and an angle of $\psi = 21°$ is reached at maximum. From all observa-
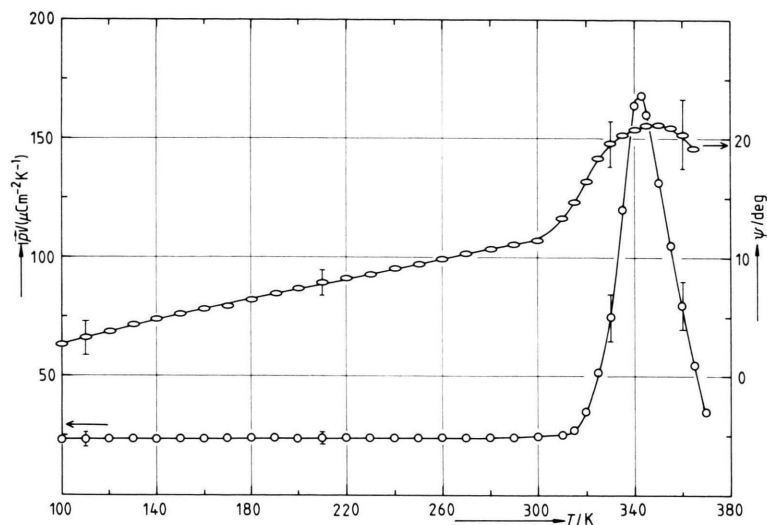
Fig. 7. Absolute value $|p|$ (○) and direction ψ (○) of the pyroelectric coefficient of 1-CN-4-Br-C$_6$H$_4$ vs. temperature.
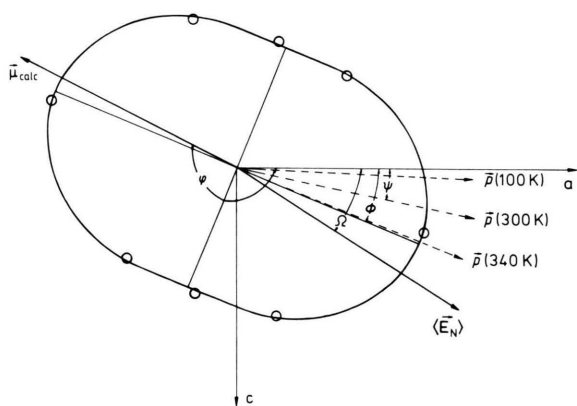

Fig. 8. Dielectric ellipse, $\varepsilon(\theta)$ (○), and pyroelectric vector, p (the sign of p is unknown) of 1-CN-4-Br-C$_6$H$_4$, together with μ_{calc} and $\langle E_N \rangle$.

Table 1. Dielectric constants and pyroelectric coefficients of 1-Cl-3-NO$_2$-C$_6$H$_4$ (CNB), 1-CN-4-NO$_2$-C$_6$H$_4$ (NBN), and 1-CN-4-Br-C$_6$H$_4$ (BBN) for selected temperatures.

T/K	CNB	NBN	BBN	
ε_i				
200 K	$\varepsilon_{33} = 3.61$	$\varepsilon_{22} = 3.43$	$\varepsilon_{11} = 3.14$,	$\varepsilon_{13} = 0.52$,
			$\varepsilon_{33} = 4.17$,	$\varepsilon_{22} = 3.38$
300 K	$\varepsilon_{33} = 4.00$	$\varepsilon_{22} = 3.90$	$\varepsilon_{11} = 3.14$,	$\varepsilon_{13} = 0.52$,
			$\varepsilon_{33} = 4.17$,	$\varepsilon_{22} = 3.38$
$|p_i|/\mu C\ m^{-2}\ K^{-1}$				
100	$p_3 = 6.2$	$p_2 = 0.32$	$p_1 = 23.6$,	$p_3 = 1.1$
180	$p_3 = 7.5$	$p_2 = 0.35$	$p_1 = 23.8$,	$p_3 = 2.8$
260	$p_3 = 8.7$	$p_2 = 0.45$	$p_1 = 23.7$,	$p_3 = 4.1$
340		$p_2 = 0.86$	$p_1 = 164.0$,	$p_3 = 5.2$

tions combined, we conclude that a reversible phase transition of the order-disorder type occurs at $T_c = T_{max} \cong 340$ K, which is accompanied by a very small enthalpy of transition. The assumption of an order-disorder transition of BBN is supported by the fact that it is chemically and structurally related to 1-Cl-4-Br-C$_6$H$_4$, which is known to be disordered in the solid state [9–11].

In Table 1 the obtained values for the dielectric constants and pyroelectric coefficients of the three substances under investigation are given for selected temperatures. In Fig. 8 the dielectric ellipse in the ac-plane is shown for BBN. Additionally the direction of the pyroelectric coefficient is plotted for $T = 100$ K, 300 K, and 340 K. By comparison of the dielectric ellipse with a schematic display of the structure of BBN in Fig. 9, it is seen that the principle axis of the ellipse is nearly parallel to the direction [101]. The direction of the pyroelectric coefficient drifts with increasing temperature towards [101], too.

Dipole Moments

Experimental dipole moments of CNB, NBN, and BBN have been reported by McClellan [12] as determined in the gaseous state and/or in solutions. We have calculated the charge distributions of the

Table 2. Calculated charge distributions, in units of the elementary charge, for $1\text{-Cl-}3\text{-NO}_2\text{-C}_6\text{H}_4$ (CNB), $1\text{-CN-}4\text{-NO}_2\text{-C}_6\text{H}_4$ (NBN), and $1\text{-CN-}4\text{-Br-C}_6\text{H}_4$ (BBN).

CNB		NBN		BBN	
C(1)	0.32	C(1)	0.12	C(1)	− 0.08
C(2)	− 0.28	C(2)	− 0.15	C(2)	− 0.08
C(3)	0.01	C(3)	− 0.06	C(3)	− 0.24
C(4)	− 0.20	C(4)	− 0.12	C(4)	0.16
C(5)	− 0.05	C(5)	− 0.07	C(5)	− 0.24
C(6)	− 0.30	C(6)	− 0.15	C(6)	− 0.08
H(C2)	0.20	H(C2)	0.16	H(C2)	0.15
H(C4)	0.19	H(C3)	0.17	H(C3)	0.16
H(C5)	0.15	H(C5)	0.16	H(C5)	0.16
H(C6)	0.15	H(C6)	0.16	H(C6)	0.15
Cl	− 0.07	C(7)	0.03	C(7)	− 0.16
		N(C7)	− 0.14	N(C7)	0.08
N(C3)	1.14	N(C4)	1.15	Br	0.02
O(1, N)	− 0.62	O(1, N)	− 0.65		
O(2, N)	− 0.64	O(2, N)	− 0.61		

Table 3. Experimental and calculated dipole moments and the electric field at the site of a reference molecule R created by the neighbouring molecules for $1\text{-Cl-}3\text{-NO}_2\text{-C}_6\text{H}_4$ (CNB), $1\text{-CN-}4\text{-NO}_2\text{-C}_6\text{H}_4$ (NBN), and $1\text{-CN-}4\text{-Br-C}_6\text{H}_4$ (BBN).

	CNB	NBN	BBN
$\lvert \boldsymbol{\mu}_{lit} \rvert \cdot 10^{30}/\text{C m}$ [12]	10.7 − 14.3	0.0 − 2.4	8.9
$\lvert \boldsymbol{\mu}_{calc} \rvert \cdot 10^{30}/\text{C m}$ *	16.9	9.1	6.7
$\mu_{calc, P} \cdot 10^{30}/\text{C m}$	11.9	7.1	6.0
$\lvert \langle E_{N, P} \rangle \rvert \cdot 10^{-9}/(\text{V m}^{-1})$ **	2.830	1.079	0.5204

 * The angle between $\boldsymbol{\mu}_{calc}$ and [100] for BBN is $\varphi = 207°$.
** The angle between $\langle \boldsymbol{E}_N \rangle$ and [100] for BBN is $\Omega = 32°$.

three substances under investigation and therefrom the dipole moments for the solid state by the quantum chemical INDO-SCEF method introduced in [6]. Semiempirical molecular orbital (MO)-calculations have been employed in an intermediate neglect of differential overlap (INDO)-type-approximation; intermolecular interactions have been simulated in a self-consistent electric field (SCEF) approach. The electric field was created in the cases of CNB and NBN by 10 and in the case of BBN by 14 neighbouring molecules. The resulting charge distributions are given in Table 2. The atomic numbering schemes used are displayed in Fig. 10 a – c.

In Table 3 the dipole moments obtained from the calculated charge distributions, $\lvert \boldsymbol{\mu}_{calc} \rvert$, are given together with the component of the dipole moment in the direction of the polarisation, $\mu_{calc, P}$. Additionally
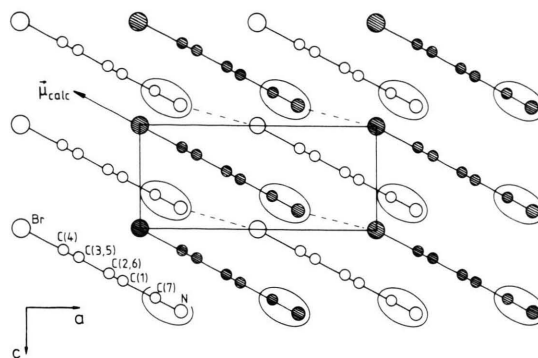

Fig. 9. Schematic display of the molecular arrangement of $1\text{-CN-}4\text{-Br-C}_6\text{H}_4$ along the axis [010]. The hatched molecules are in the plane $(a\,0\,c)$, the other ones in the plane $(a\,\tfrac{1}{2}\,c)$.

for BBN, symmetry m, the angle between $\boldsymbol{\mu}$ and the axis [100] (φ) is given in this table. For comparison we have also listed the dipole moments reported by McClellan $\lvert \boldsymbol{\mu}_{lit} \rvert$. In the cases of CNB and BBN, $\lvert \boldsymbol{\mu}_{calc} \rvert$ is in satisfactory agreement with $\lvert \boldsymbol{\mu}_{lit} \rvert$, if the accuracy of the experimental and calculated values is considered [6, 12]. In the case of NBN a summation of uncertainties in the quantum chemical calculations obviously leads to a much to high a value of $\lvert \boldsymbol{\mu}_{calc} \rvert$. This probably occurs because the dipole moment of NBN results mainly from the difference in the partial dipole moments due to groups with comparable electron withdrawing effects in opposite direction.

From the charge distribution and the crystal structure data [2 − 4], we have calculated the electric field $\boldsymbol{E}_N(x, y, z)$ created by the neighbouring molecules N at the site of a reference molecule R [6, 7],

$$E_N(x, y, z) = \frac{1}{4\pi\,\varepsilon_0} \sum_N \sum_j \frac{q_j \cdot \boldsymbol{r}_j}{\lvert \boldsymbol{r}_j \rvert^3} \equiv \frac{1}{4\pi\,\varepsilon_0} \boldsymbol{S}_N(x, y, z) \tag{1}$$

with $\boldsymbol{r}_j$ = radius vector from atom j in the external molecule N to the reference unit R, q_j = charge of atom j, and $\boldsymbol{S}_N$ = abbreviation for the summation. $E_N(x, y, z)$ was averaged over the volume of the reference molecule V_R, leading to

$$\langle E_N \rangle = \frac{1}{V_R} \sum E_N(x, y, z)\, \Delta V \equiv \frac{1}{4\pi\,\varepsilon_0} \langle \boldsymbol{S}_N \rangle. \tag{2}$$

In the cases of CNB, NBN, and BBN 70, 94, and 126 neighbouring molecules, respectively, are used to create the electric field. The resulting values for $\langle E_N \rangle$ and $\langle E_{N, P} \rangle$ = component of $\langle E_N \rangle$ in the direc-

tion of polarisation, are given in Table 3. For BBN the angle, Ω, between $\langle E_N \rangle$ and the axis [100] is listed, too. It can be seen from Figs. 8 and 9 that the direction of the dipole moment of BBN coincides with the molecular axis.

Discussion

The three substances, m-chloronitrobenzene, CNB, p-nitrobenzonitrile, NBN, and p-bromo-benzonitrile, BBN, show comparable dielectric properties with $3 < \varepsilon' < 4.5$ in the whole temperature range studied. However the temperature dependences $d\varepsilon'/dT$ are different. On the other hand strong differences appear in the pyroelectric properties with $0.3 < |p|/(\mu C\ m^{-2}\ K^{-1}) < 170$. These variations do not parallel the diverse dipole moments of the three substances. In the case of NBN it is true that an almost negligible dipole moment is accompanied by a very small $|p|$. In case of CNB and BBN, however, $|\mu|(CNB) > |\mu|(BBN)$, while $|p|(CNB) < |p|(BBN)$ (see Table 3).

In a detailed discussion [6, 7] it was shown that the temperature dependence of the polarization P, e.g. the value of the pyroelectric coefficient p, can be calculated as a function of molecular and crystal properties, $p = f(\varepsilon_P, \alpha, \mu, E_L, E_N)$ with $\alpha =$ dipole polarizability and $E_L =$ Lorentz field [8]. The resulting equation for the pyroelectric coefficient in the employed model is

$$p = \frac{dP}{dT} = \frac{N_A}{3\bar{V}}(\varepsilon_p + 2) \cdot |\mu| \cdot \frac{d\cos\delta}{dT}$$
$$+ \frac{1}{4\pi}(\varepsilon_p - 1) \cdot |\langle S_N \rangle| \cdot \frac{d\cos\beta}{dT}$$
$$+ \left(\frac{N_A}{3\bar{V}} \cdot |\mu| \cdot \cos\delta + \frac{1}{4\pi} \cdot |\langle S_N \rangle| \cdot \cos\beta\right) \frac{d\varepsilon_p}{dT}$$
$$= p_I + p_{II} + p_{III} \tag{3}$$

with $1/\bar{V} = \varrho/M =$ number of molecules per unit volume, $\varrho =$ mass density, $M =$ molar mass, $N_A =$ Avogadro number, $\varepsilon_p =$ dielectric constant in the direction of P, $\delta = \measuredangle(\mu, P)$, and $\beta = \measuredangle(\langle E_N \rangle, P)$. In (3) the temperature dependence of the crystal volume is already neglected, i.e. $\bar{V} =$ const in the temperature range considered.

In case of CNB and NBN ε_P corresponds to ε_{33}(CNB) and ε_{22}(NBN), respectively. Values for ε_P can be found in Figs. 1 and 2; $d\varepsilon_p/dT$ can be
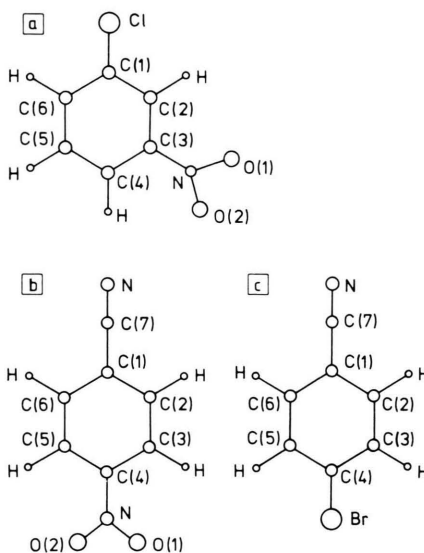
Fig. 10. Atomic numbering scheme of a) 1-Cl-3-NO$_2$-C$_6$H$_4$, b) 1-CN-4-NO$_2$-C$_6$H$_4$, and c) 1-CN-4-Br-C$_6$H$_4$.

extracted therefrom. The variation of $\cos\delta$ and $\cos\beta$ with temperature, originating in a change of molecular dipole librational motions, can be described by a classical harmonic oscillator model [1, 13]:

$$\frac{d\cos\delta}{dT} = -\frac{\cos\delta}{2T}(J_0(\Phi_{x'})J_1(\Phi_{y'})\Phi_{y'}$$
$$+ J_0(\Phi_{y'})J_1(\Phi_{x'})\Phi_{x'}). \tag{4}$$

$J_0(\Phi_i)$, $J_1(\Phi_i)$, $i = x', y' =$ Bessel functions of first kind and zero order, and of first kind and first order, respectively, $\Phi_{x'}, \Phi_{y'} =$ amplitudes of the dipole oscillations about the principal molecular axes x' and y'. The z'-axis defines the direction of the dipole moment while x' and y' are lying in a plane perpendicular to the z'-axis. By classical harmonic approximation the mean square amplitude of libration about each axis is

$$\Phi_i = \left(\frac{kT}{2\pi^2 v_i^2 I_i}\right)^{1/2}. \tag{5}$$

$I_i =$ moment of inertia, $v_i =$ librational frequency of the dipole around the axis i. For $\Phi_i < 0.4$ there is $J_0 \cong 1$ and $J_1 \cong \Phi_i/2$ in good approximation, e.g. with an accuracy of 4%. Combining (4) and (5) and taking this approximation into account, leads to

$$\frac{d\cos\delta}{dT} = -\cos\delta \frac{k}{8\pi^2}\left(\frac{1}{v_{x'}^2 I_{x'}} + \frac{1}{v_{y'}^2 I_{y'}}\right). \tag{6}$$

Table 4. Calculated pyroelectric coefficients for 1-Cl-3-NO$_2$-C$_6$H$_4$ (CNB), 1-CN-4-NO$_2$-C$_6$H$_4$ (NBN), and 1-CN-4-Br-C$_6$H$_4$ (BBN) at selected temperatures.

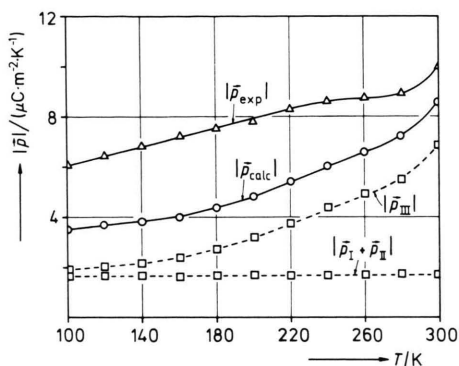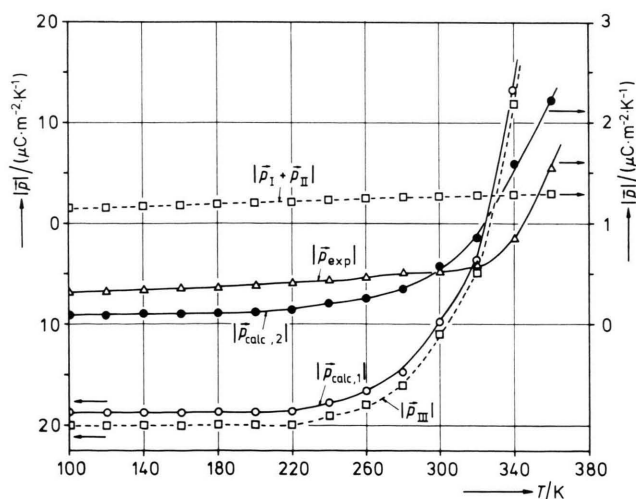| T/K	$|p_{calc}|/(\mu C\ m^{-2}\ K^{-1})$		
	CNB	NBN	BBN
100	3.5	18.8	14.4
180	4.4	18.8	12.9
260	6.6	16.8	13.0
340		13.3	6.5

Fig. 11. Calculated pyroelectric coefficients $|p_{calc}|$ (○), $|p_I + p_{II}|$ (□), and $|p_{III}|$ (□), together with the measured one $|p_{exp}|$ (△) for 1-Cl-3-NO$_2$-C$_6$H$_4$ vs. temperature.

This means that d cos δ/dT is constant in the whole temperature range. Since $\beta = \delta + 180°$, d cos β/dT is equal to $-$ d cos δ/dT.

Raman spectroscopic data are reported for CNB [14–16]. Therefrom the values of $\tilde{v}_{x'}$(CNB) = 25 cm^{-1} and $\tilde{v}_{y'}$(CNB) = 59 cm^{-1} have been adopted for the frequencies of molecular librational motions of CNB. The principle moments of inertia $I_{x'}$(CNB) = $1.57 \cdot 10^{-44}$ kg m^2 and $I_{y'}$(CNB) = $1.20 \cdot 10^{-44}$ kg m^2 are given in [14], too. No spectroscopic data are available for NBN. In a first approximation the values of d cos δ/dT for CNB have been adopted for NBN. This makes sense, since the molecular structure and the moments of inertia, respectively, of CNB and NBN are comparable; $I_{x'}$(NBN) = 1.64 $\cdot 10^{-44}$ kg m^2 and $I_{y'}$(NBN) = $1.43 \cdot 10^{-44}$ kg m^2. With d cos δ/dT and d cos β/dT found in this way and with $\mu_{calc, P}$ and $\langle E_{N, P} \rangle$ resulting from the quantum chemical calculations, p(CNB) = $f(T)$ and p(NBN) = $f(T)$ result. $|p_{calc}|$(CNB) = $f(T)$ and $|p_{calc}|$(NBN) = $f(T)$ are shown in Figs. 11 and 12, respectively. The components ($|p_I + p_{II}|$) and $|p_{III}|$ corresponding to the three terms in (3) are given in these figures, too. Additionally the experimental values $|p_{exp}|$ are plotted. For selected temperatures $|p_{calc}|$ is listed in Table 4.

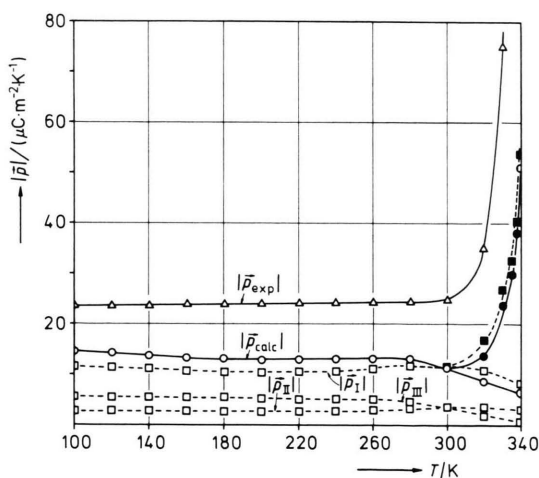In case of CNB fair agreement between the calculated and the measured pyroelectric coefficient

Fig. 12. Calculated pyroelectric coefficients $|p_{calc}|$ (○, ●), $|p_I + p_{II}|$ (□), and $|p_{III}|$ (□), together with the measured one $|p_{exp}|$ (△) for 1-CN-4-NO$_2$-C$_6$H$_4$ vs. temperature.

Fig. 13. Calculated pyroelectric coefficients $|p_{calc}|$ (○), $|p_I|$ (□), $|p_{II}|$ (□), and $|p_{III}|$ (□), together with the measured one $|p_{exp}|$ (△) for 1-CN-4-Br-C$_6$H$_4$ vs. temperature. Filled symbols represent data calculated with the assumption of onset of molecular librational motions at $T > 300$ K.

is found, while for NBN the misfit is substantial. The fact is, that in both cases the accuracy of μ and $\langle E_N \rangle$ is not better than 20% [6]. By chance the uncertainties in μ(CNB) and $\langle E_N \rangle$(CNB) cancel each other, but they accumulate for NBN. The third term in (3), p_{III}, is mainly due to the difference in $|\mu|$ and $|\langle E_N \rangle|$. It is obvious that the uncertainties in $|\mu|$ and $|\langle E_N \rangle|$ multiply in p_{III}. An empirical value of $1.4 \cdot |\langle E_N \rangle|$ (NBN) leads to $|p_{calc,2}|$, which fits the experimental curve satisfactory. Despite of this, both values $|\mu|$(NBN) and $1.4 \cdot |\langle E_N \rangle|$ (NBN) resulting from the calculated charge distribution, show still much to high values. It can be seen that uncertainties introduced by the quantum chemical calculations affect the model used to calculate $p = f(T)$ heavily if μ and $\langle E_N \rangle$ are influenced in a different way.

For BBN the angular variation of the polarization P with T was calculated from

$$P = \int p(T)\, dT, \qquad (7)$$

using the measured pyroelectric coefficient and $P = 0\ \mu C\ m^{-2}\ K^{-1}$ for $T > T_c$ as starting point for the integration. Thereby we assume that the phase transition leads to a non polar structure. The direction of the polarization, P(BBN), is not fixed along a crystal axis but can point in any direction within the ac-plane. The direction of P(BBN) must be known for a proper estimate of $\varepsilon_P = f(T, \theta)$ from the measured values. Furthermore the changes of δ and β with temperature are deduced directly from the angular variation of $P = f(T)$, assuming μ and $\langle E_N \rangle$ to be constant over the whole temperature range. Therefore (4) and (5) are not needed for the calculations.

$|p_{calc}|$(BBN) $= f(T)$ and $|p_{exp}|$(BBN) are shown in Fig. 13 together with the components $|p_I|$, $|p_{II}|$, and $|p_{III}|$. The latter ones correspond to the appropriate terms in (3). $|p_{calc}|$ turnes out to be considerably smaller than $|p_{exp}|$. However the practical independence of $|p_{exp}|$ from temperature is reflected by $|p_{calc}|$ in the temperature range $100 \leqq T/K \leqq 300$. Selected values of $|p_{calc}| = f(T)$ are given in Table 4.

The very strong increase of $|p_{exp}|$ near T_c can not be explained in the light of $\varepsilon(T) = f(T)$, $\delta(T) = f(T)$, and $\beta(T) = f(T)$, but it can be interpreted by taking the molecular processes at T_c into account. A schematic display of the crystal structure of BBN [4] is shown in Figure 9. The possibility that molecular librational motions increase with increasing temperature has to be considered. For example, a change of the mean molecular direction due to librational motions about the axis [010] is equivalent to a change in the direction of the dipole moment. Due to the variation of $\cos \delta$, where $\delta = \measuredangle (\mu, P)$, this would affect the first term in (3). So a structural change directly gives rise to a change in the pyroelectric coefficient.

The curves represented by filled symbols in Fig. 13 are calculated using a change in direction of μ from $\varphi = 207°$ to $\varphi = 203°$ in the temperature range $320 \leqq T/K \leqq 340$. Thereby the assumption was made that $d\delta/dT$ increases with $T \to T_c$. In this way the increase of the measured pyroelectric coefficient can be interpreted as an increase of molecular librational motions about the axis [010], leading to a change of the mean direction of the dipole moments.

On the other hand librational motions about the axis perpendicular to the molecule plane are possible. A setting in of an order-disorder mechanism at about T_c due to a 180° flip about this axis is thinkable. Such a mechanism would lead to a decrease of the averaged value of $|\mu|$ and $|\langle E_N \rangle|$ and therefore to a decrease of $|p_I|$ and $|p_{II}|$ in (3). Therefore the 180° flip of the molecules about an axis perpendicular to the molecule plane might be an explanation for the decrease of $|p_{exp}|$ for $T > T_c$.

[1] T. Asaji and Al. Weiss, Z. Naturforsch. **40a,** 567 (1985).
[2] S. Sharma, H. Paulus, N. Weiden, and Al. Weiss, Z. Kristallogr. **171,** 101 (1985).
[3] T. Higashi and K. Osaki, Acta Crystallogr. **B 33,** 2337 (1977).
[4] D. Britton, J. Konnert, and S. Lam, Cryst. Struct. Comm. **6,** 45 (1977).
[5] D. Berlincourt, W. R. Cook, and M. E. Rander, Acta Crystallogr. **16,** 163 (1963).
[6] S. Fleck, M. C. Böhm, and Al. Weiss, Z. Naturforsch. **42a,** 57 (1987).
[7] S. Fleck and Al. Weiss, Z. Naturforsch. **41a,** 1289 (1986).
[8] J. F. Nye, Physical Properties of Crystals. Clarendon Press, Oxford 1957.
[9] S. B. Hendricks, Z. Kristallogr. **84,** 85 (1933).
[10] A. Klug, Nature London **160,** 570 (1947).
[11] C. Dean, J. Chem. Phys. **23,** 1734 (1955).
[12] A. L. McClellan, Tables of Experimental Dipole Moments. Freeman, San Francisco 1963.
[13] F. J. Mopsik and M. G. Broadhurst, J. Appl. Phys. **46,** 4202 (1975).
[14] N. Le Calve, F. Romain, and B. Pasquier, J. Raman Spectrosc. **8,** 239 (1979).
[15] C. Pigenet, N. Le Calve, and B. Pasquier, J. Raman Spectrosc. **9,** 393 (1980).
[16] C. Pigenet, N. Le Calve, and B. Pasquier, J. Mol. Struct. **61,** 183 (1980).